An Enhanced Finite Element Model for Determination of Load Capacity in Planetary Gear Trains

Ignacio Gonzalez-Perez, Alfonso Fuentes and Kenichi Hayasaka

Abstract Planetary gear trains are being intensively applied in automobile drivelines during recent years due to its high load capacity, compact size, high gear ratio, and axial direction of power path. Determination of the load capacity in the design stage requires the calculation of contact pressures and bending stresses at the ring, sun, and planet gears. The knowledge of the load sharing between the planet gears and how it is affected by any assembly error or by the deflection of supporting shafts and carrier is needed for the determination of tolerances before manufacturing and assembly stages are accomplished. An enhanced finite element model is presented in this paper for the purpose of determination of the load capacity in planetary gear trains and investigation of the load sharing between the planet gears. A numerical example is presented.

Keywords Planetary gear trains · Stress analysis · Finite element method

1 Introduction

Planetary gear trains are being intensively applied in automobile drivelines during recent years and have been an object of intensive research [1–4]. The knowledge of the load sharing between the planet gears and how it is affected by any assembly

F2012-C02-008

I. Gonzalez-Perez (✉) · A. Fuentes
Polytechnic University of Cartagena (UPCT), Cartagena, Spain
e-mail: ignacio.gonzalez@upct.es

K. Hayasaka
Space Creation Co. Ltd, Hamamatsu, Japan

SAE-China and FISITA (eds.), *Proceedings of the FISITA 2012 World Automotive Congress*, Lecture Notes in Electrical Engineering 193,
DOI: 10.1007/978-3-642-33744-4_11,

error or by the deflection of supporting shafts and carrier is needed for the determination of the actual load capacity.

An enhanced finite element model is presented in this paper for the purpose of determination of the load capacity in planetary gear trains and investigation of the load sharing between the planet gears. The finite element model is built from the designed bodies of the sun, the ring, and the planet gears. Besides the gear bodies, the carrier body and the supporting shafts are included into the model.

The presented research work has been performed through the following steps:

(1) Computerized generation of the gear geometry corresponding to the sun gear, the ring gear, and the planet gears. Involute tooth surface equations and portions of the corresponding rims are considered in the determination of the designed bodies.
(2) Assembly of the sun gear, the ring gear, and the planet gear bodies for different contact positions.
(3) Determination of the designed bodies of the carrier and the supporting shafts.
(4) Automatic generation of the finite element model for the planetary gear train.
(5) Determination of contact and bending stresses at the gear teeth.
(6) Determination of stresses and deformations in the carrier and supporting shafts.

The presented enhanced finite element model constitutes a step forward in the design of planetary gear trains since: (1) the mesh of the gear bodies is automatically generated for any design data, (2) the modelling of the gear shafts and the carrier is included, (3) the boundary and load conditions can be easily adapted to the working conditions of this type of gear drives, and (4) a different design of the carrier can be easily integrated into the model.

2 Computerized Generation of Gear Geometry and Assembly

Generation of gear tooth surfaces is a well-known topic in theory of gearing [5]. For the determination of the geometry of each gear of the planetary gear train, involute profiles are considered for the active parts of the gear tooth surfaces.

The geometry of the gear tooth surfaces for gears 1 (the sun gear), 2 (the planet gear), and 3 (the ring gear) are obtained computationally. Figure 1 shows the normal sections of three teeth, each one corresponding to the sun gear, the planet gear, and the ring gear, respectively.

The assembly of the planetary gear train requires the determination of the phase angles $\mu_2^{(k)}$ of the planet gears (see Fig. 2). Here, the index 2 refers to any planet gear and the index k, $k = \{1, \ldots, n\}$, refers to a specific planet gear, where n is the number of planet gears. The phase angles are determined as [5]

$$\mu_2^{(k)} = -\delta_1^{(k)} \cdot \frac{N_1}{N_2}$$

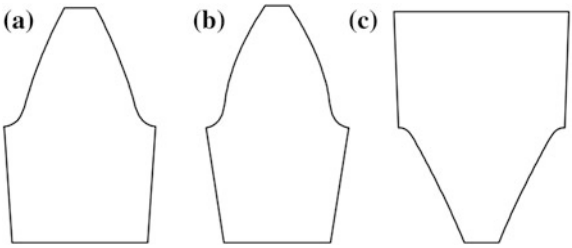

Fig. 1 Illustration of the normal sections of **a** a sun gear, **b** a planet gear, and **c** a ring gear tooth

or

$$\mu_2^{(k)} = \delta_3^{(k)} \cdot \frac{N_3}{N_2}$$

Here, N_1, N_2, and N_3 are the tooth number of the sun, the planet, and the ring gears, respectively. Angles $\delta_1^{(k)}$ and $\delta_2^{(k)}$ are determined as

$$\delta_1^{(k)} = m_1^{(k)} \cdot \frac{2\pi}{N_1} - \frac{2\pi}{n}(k-1)$$

$$\delta_3^{(k)} = m_3^{(k)} \cdot \frac{2\pi}{N_3} - \frac{2\pi}{n}(k-1)$$

where $m_1^{(k)}$ and $m_2^{(k)}$ are obtained as

$$m_1^{(k)} = NINT\left[(k-1) \cdot \frac{N_1}{n}\right]$$

$$m_3^{(k)} = NINT\left[(k-1) \cdot \frac{N_3}{n}\right]$$

Here, the function *NINT* provides the nearest integer value of the argument. A positive sign of the phase angles means a counter-clockwise rotation of the reference axis of the planet gear respect to its initial position.

Figure 2 shows the assembly of the planetary gear train where three-tooth designed bodies are identified by means of dark lines. Such designed bodies are considered later in the finite element model generation of the planetary gear train.

3 Finite Element Model Generation

The finite element model is built with the designed bodies represented in Fig. 3 and considering the assembly shown in Fig. 2.

The meshing of the designed bodies is performed automatically [5] as a function of the number of nodes in profile and longitudinal directions. Figure 4 shows the mesh of a three-tooth sun gear designed body. In the case of the sun gear

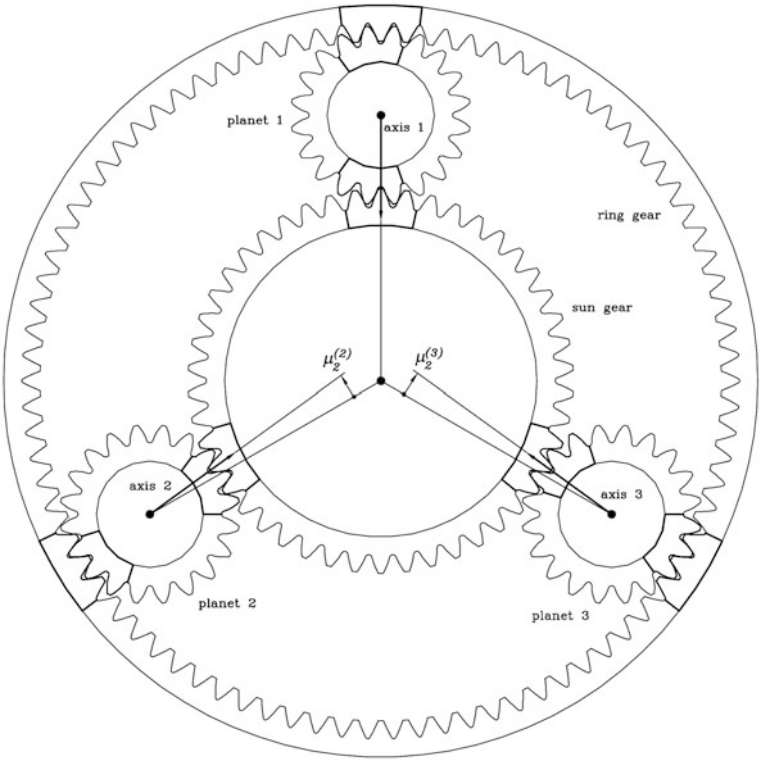

Fig. 2 Assembly of the planet gears in the planetary gear train

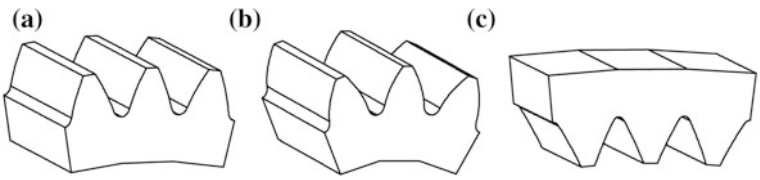

Fig. 3 The designed bodies for: **a** the sun gear, **b** the planet gear, and **c** the ring gear

or the ring gear, a total of n three-tooth designed bodies are considered, where n is the number of planet gears. In the case of the planet gears, two three-tooth designed bodies are considered for each planet gear, one in contact with the sun gear model and the other one in contact with the ring gear model.

Two configurations of the finite element model have been considered for the planetary gear train. The first configuration named as *rigid* configuration assumes an infinite value of the coefficient of rigidity for the carrier and supporting shafts of the planets. The second configuration named as *flexible* configuration assumes a coefficient of rigidity according to the modelled carrier and supporting shafts of the planets.

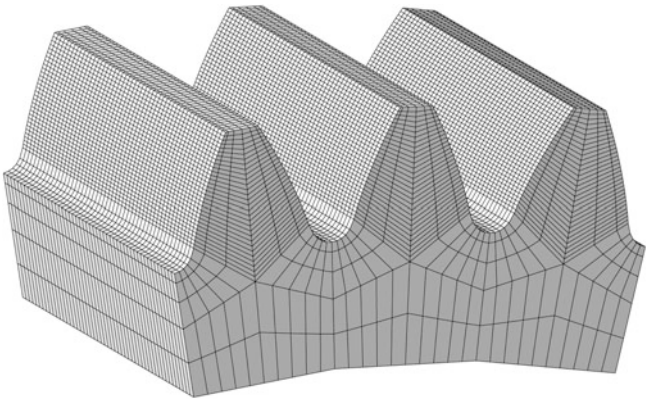

Fig. 4 The finite element meshing of a three-tooth designed body for the sun gear model

In the case of the *rigid* configuration, the boundary conditions are applied as follows (see Fig. 5):

(1) Nodes on the two sides and the bottom part of the sun gear rims, the planet gear rims, and the ring gear rims, form rigid surfaces S_{1i}, S_{2ia}, S_{2ib}, and S_{3i}, where $i = \{1, \ldots, n\}$.
(2) Reference nodes N_{1i}, N_{2ia} and N_{2ib}, and N_{3i}, located on the axes of the sun gear, the planet gear, and the ring gear, respectively, are used as the reference points of the previously defined rigid surfaces.
(3) Rigid surfaces S_{2ia} and S_{2ib} are rigidly connected to reference nodes N_{2ia} and N_{2ib}, respectively. Each node N_{2ib} is connected to a node N_{2ia} for each planet gear through a *weld* connection [6]. The whole set constitutes one rigid body for each planet gear and its boundary conditions are defined at each node N_{2ia}, $i = \{1, \ldots, n\}$.
(4) Rigid surfaces S_{1i} are rigidly connected to reference nodes N_{1i}, $i = \{1, \ldots, n\}$, that are connected each other through a *weld* connection [6]. The n three-tooth designed bodies of the sun gear constitute one rigid body where the boundary and load conditions are defined at node N_{11}.
(5) Rigid surfaces S_{3i} are rigidly connected to reference nodes N_{3i}, $i = \{1, \ldots, n\}$, that are connected each other through a *weld* connection [6]. The n three-tooth designed bodies of the ring gear constitute one rigid body where the boundary and load conditions are defined at node N_{31}.
(6) Boundary conditions for the stress analysis of the planetary gear train are applied to the inverted mechanism of the planetary gear train where the carrier is fixed and the ring gear is free to rotate.
(7) At each contact position, sun, planet and ring gear models are installed in a fixed reference system considering their angular positions, which are obtained from the gear ratios and the phase angles.

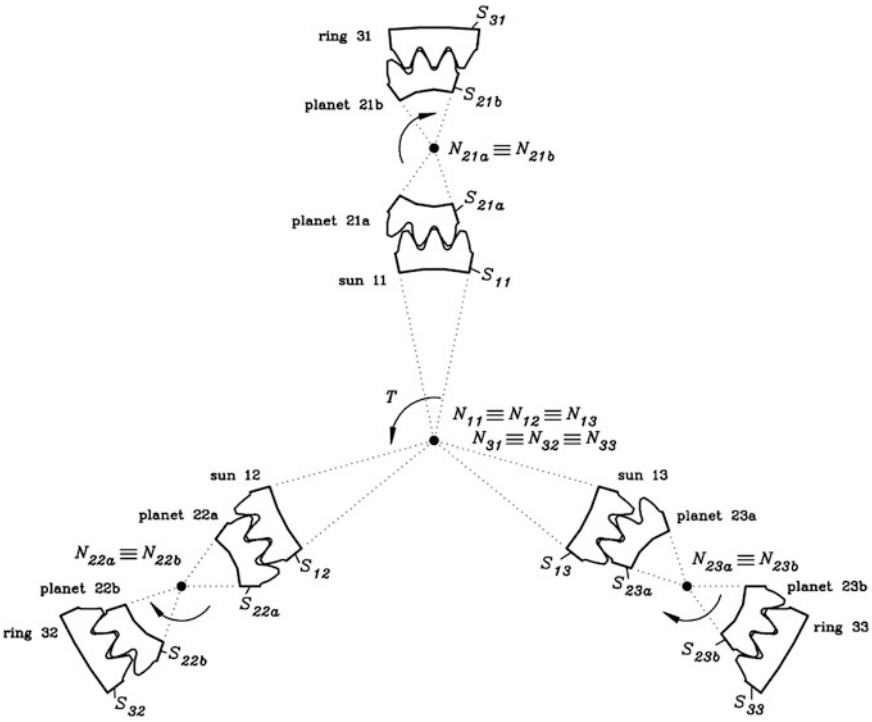

Fig. 5 For application of the boundary conditions at the *rigid* configuration of the planetary gear train

(8) For the stress analysis at a given contact position, all the degrees of freedom of reference node N_{31} are restricted, whereas nodes N_{11} and N_{2ia}, $i = \{1, \ldots, n\}$, are just free to rotate about the sun and the planet axes, respectively.
(9) A torque T is applied at the free rotational motion of reference node N_{11} and this allows the load to be transmitted to the sun gear model through the rigid surfaces S_{1i}, $i = \{1, \ldots, n\}$.
(10) Each planet gear model, which can rotate freely around its planet axis, is loaded by the push of the sun gear model and by the blocked ring gear model.

In the case of a *flexible* configuration, some differences are incorporated to the finite element model respect to the *rigid* configuration (see Figs. 6 and 7):

(1) The planet gear models are provided with their corresponding shafts, which are modelled by beam elements. Nodes N_{2ia}, $i = \{1, \ldots, n\}$, are connected to a node of the corresponding planet shaft by means of a *hinge* connection [6]. This means that the designed bodies of the planet gears can freely rotate around their axes.

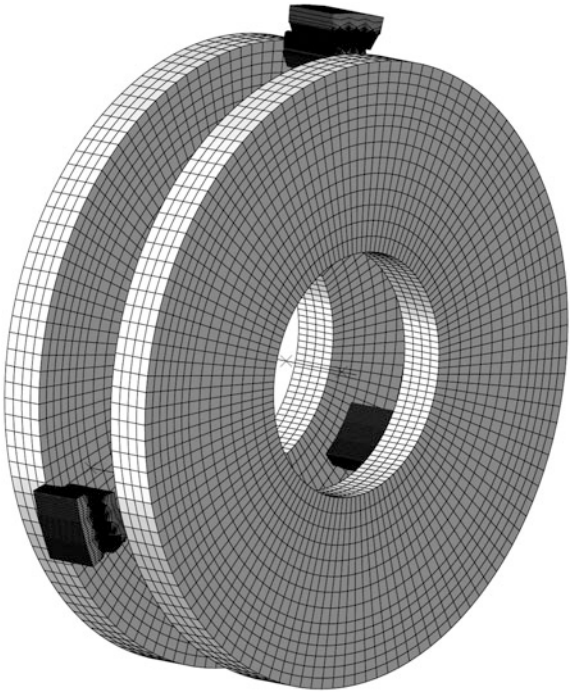

Fig. 6 A *flexible* configuration for the planetary gear train

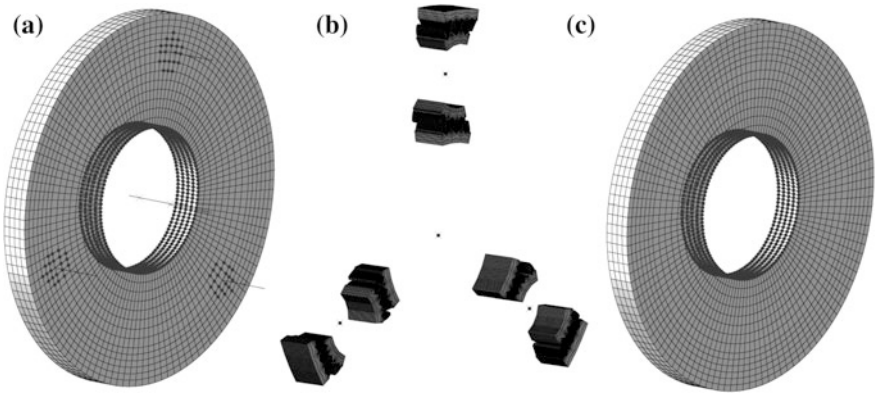

Fig. 7 *Flexible* configuration parts of a planetary gear train: **a** disk 1 of the carrier, planet shafts and carrier shaft, **b** gears, and **c** disk 2 of the carrier

(2) The carrier is incorporated to the finite element model by means of two disk-shape bodies and one shaft. A set of nodes on the inner surfaces of both disks are rigidly connected to two nodes on the carrier shaft.

Table 1 Basic design data of the planetary gear train

	Sun gear	Planet gear	Ring gear
Number of teeth	46	20	86
Module [mm]		2.0	
Pressure angle [degrees]		25.0	
Profile shift coefficient	−0.2408	+0.1052	+0.03
Face width [mm]		15.0	
Centre distance [mm]		65.7873	
Input torque [Nm]	200.0		

(3) Each planet shaft is rigidly connected to the carrier through both end nodes using a *weld* connection [6] between each end-node and a predefined set of nodes on the face of the carrier disks.
(4) The rotation of the carrier shaft is blocked while a torque T is applied to the sun gear reference node N_{11}.

Figure 6 shows the finite element model of a *flexible* configuration for the planetary gear train. Figure 7 shows the *flexible* configuration parts based on the two disk-shape bodies of the carrier, the planet and carrier shafts, and the gears.

4 Numerical Example

A planetary gear train based on $n = 3$ planet gears is considered for stress analysis. The main design data for such a train is shown in Table 1. The required phase angles for the assembly of the planetary gear train (see Fig. 2) are shown in Table 2.

A total of four configurations of the planetary gear train are considered for stress analysis. The main data for such configurations are shown in Table 3. The *rigid* configuration has a total of 414007 elements and 504912 nodes. The *flexible* configuration has a total of 427576 elements and 523036 nodes. A Young's module is 207 GPa and a Poisson's ratio of 0.29 are considered.

Two types of assembly errors of the planet gears on the carrier are considered for stress analysis. Figure 8 shows a possible tangential assembly error Δt and a possible radial assembly error Δr of planet gear 1. The considered values of assembly errors for stress analysis are {0, 2, 4, 6, 8, 10} μm.

For each analysis, the maximum contact pressure is determined at each planet gear. Figure 9 shows a maximum contact pressure of 525.7 MPa in planet gear 1 for the case of the *rigid* configuration when no assembly errors are considered.

Figure 10 shows the evolution of maximum contact pressure at the three planet gears for different values of the tangential assembly error Δt of planet gear 1. In the case of the *rigid* configuration (Fig. 10(a)), the tangential assembly error Δt causes larger differences of contact pressures between the planet gears than in the case of a *flexible* configuration (Fig. 10(b)). Therefore, the maximum contact pressure in

Table 2 Phase angles for the assembly of planet gears in the planetary gear train

	Planet 1	Planet 2	Planet 3
$m_1^{(k)}$	0	15	31
$m_3^{(k)}$	0	29	57
$\delta_1^{(k)}$ [rad]	0	−0.045530	+0.045530
$\delta_3^{(k)}$ [rad]	0	+0.024353	−0.024353
$\mu_2^{(k)}$ [rad]	0	+0.104720	−0.104720
$\mu_2^{(k)}$ [degrees]	0	+6.0	−6.0

Table 3 Rigid and flexible configurations of the planetary gear train

	Rigid	Flexible 1	Flexible 2	Flexible 3
Planet shaft radius [mm]	∞	9.0	11.0	9.0
Disk thickness [mm]	∞	12.0	12.0	8.0

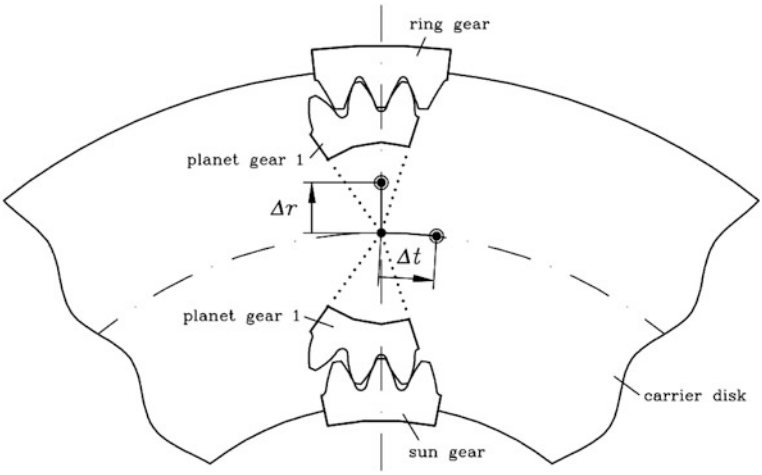

Fig. 8 Assembly errors Δt and Δr of planet gear 1 on the carrier

the planetary gear train is larger in the *rigid* configuration than in any *flexible* configuration as a consequence of a larger uneven distribution of the load between the planet gears.

Figure 11 shows the evolution of the maximum contact pressure at different configurations of the planetary gear train considering several values of the tangential assembly error Δt and the radial assembly error Δr (see Fig. 8). Figure 11a shows that the radial assembly error Δr does not cause an increment of the maximum contact pressure in the planetary gear train and therefore this type of error does not contribute to an uneven distribution of load between the planet gears. Figure 11b shows some differences between the three *flexible* configurations (see Table 3) when a tangential assembly error Δt is considered.

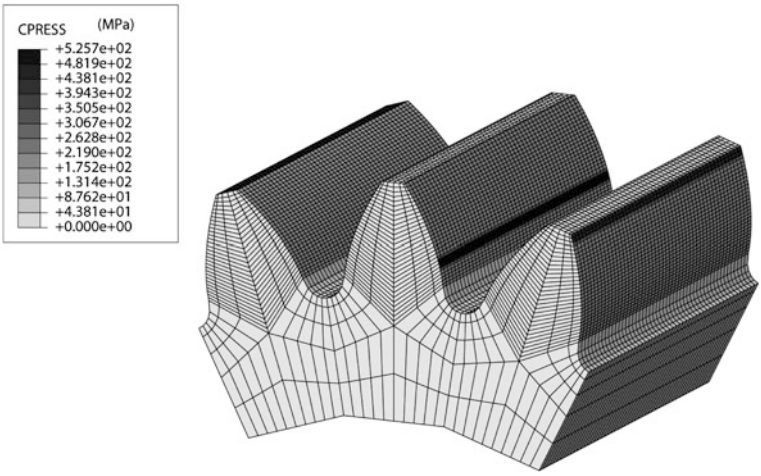

Fig. 9 Contact pressure in planet gear 1 when the *rigid* configuration and no assembly errors are considered

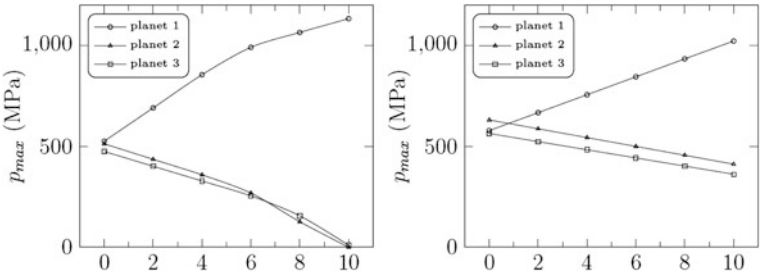

Fig. 10 Evolution of maximum contact pressure at the three planet gears for several values of Δt error in the assembly of planet gear 1 in case of **a** the rigid configuration and **b** the flexible configuration number 1

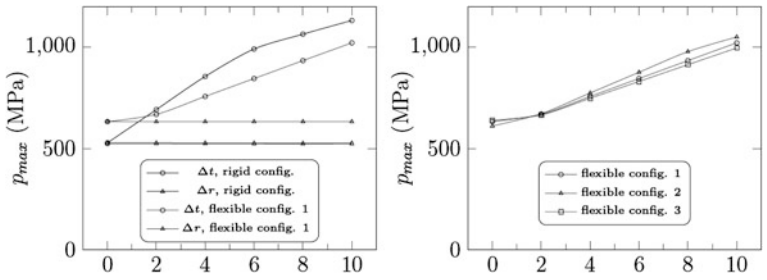

Fig. 11 Evolution of maximum contact pressure at the planetary gear train for several values of assembly errors Δt and Δr of planet gear 1 on the carrier

5 Conclusions

The developed research allows the following conclusions to be drawn:

(1) An enhanced finite element model for determination of the load capacity in planetary gear trains has been proposed.
(2) The designed bodies of the sun gear, the ring gear, the planet gears, the carrier and the supporting shafts have been included into the model.
(3) Stress analysis can be performed considering different types of assembly error of the planet gears on the carrier and different design parameters of the planetary gear train.
(4) A different design of the carrier can be easily integrated into the model.

Acknowledgments The authors express their deep gratitude to the Spanish Ministry of Economy and Competitiveness—MINECO (formerly Ministry of Science and Innovation) for the financial support of research project Ref. DPI2010-20388-C02-01 (financed jointly by *FEDER*).

References

1. Bodas A, Kahraman A (2001) Influence of manufacturing errors and design parameters on the static planet load sharing behavior of planetary gear sets. International motion and power transmission conference, Fukuoka, Japan
2. Kahraman A, Kharazi AA, Umrani M (2003) A Deformable Body Dynamic Analysis of Planetary Gears with Thin Rims. J Sound Vib 262:752–768
3. Mundo D (2006) Geometric design of a planetary gear train with non-circular gears. Mech Mach Theory 41:456–472
4. Vecchiato D (2006) Tooth contact analysis of a misaligned isostatic planetary gear train. Mech Mach Theory 41:617–631
5. Litvin F, Fuentes A (2004) Gear geometry and applied theory. Cambridge University Press, New York
6. Abaqus 6.11 user documentation, Simulia, Dassault Systèmes